JOURNAL OF MATERIALS SCIENCE 26 (1991) 163–171

Strengthening in deformation-processed Cu–20% Fe composites

Y. S. GO
329 Bokyong-ri Ilro-yeup Muan-kun Chunnam, South Korea

W. A. SPITZIG
Metallurgy and Ceramics division, Ames Laboratory-USDOE, Iowa State University, Ames, Iowa 50011, USA

Three Cu–20% Fe composites with different iron powder sizes were fabricated using powder metallurgy processes. The strengths of these composites after extensive deformation processing by rod swaging and wire drawing were shown to be anomalously higher than those predicted by rule of mixtures equations. However, the strengths obey a Hall–Petch type relationship with the iron filament spacings. The strengths of the Cu–20% Fe composites after equivalent deformation processing increased with decreasing initial iron powder size. Comparison of a Cu–20% Fe composite with a similar Cu–20% Nb composite showed that Cu–20% Fe was stronger after an identical degree of deformation processing. This increase in strength of a Cu–20% Fe composite over that of a Cu–20% Nb composite correlated with the greater shear modulus of iron compared to niobium using a barrier model for hardening.

1. Introduction

Composite materials of many types are now widely employed in industry. Composites are used to increase mechanical or physical properties, which could not be achieved by using conventional materials, by combining at least two discrete materials. Glass fibre–plastic matrix composites [1], for example, have high strength which is not attainable with bulk glass specimens.

On a geometrical basis, composites can be classified into three groups depending on whether their morphology [2] is lamellar, particulate or fibrous. The lamellar composites have a layered structure, the particulate composites have a dispersion of particles in the matrix and the fibre composites have a fibrous phase dispersed within the matrix phase. The fibre composites show the highest strength when the fibres are aligned parallel to the loading direction [3]. There are two methods for producing the aligned fibre composites [4]. The first method is to align preformed fibres and deposit the matrix around them. This method is widely used in the glass fibre–plastic matrix systems. A second method is to form fibres as integral parts of the composites during fabrication. These are called *in situ* or deformation-processed composites.

In situ composites are usually fabricated by means of powder metallurgy [5, 6], directional solidification of a fibrous eutectic [7, 8], or casting procedures such as consumable arc melting [9] or bottom casting [10]. The casting procedures are useful where two metals are insoluble in each other in the solid state. A bundle and draw process [11, 12] is also a fabrication method whereby a rod of one component is inserted into a tube of another and the resulting composite is first drawn into wire, and then cut into suitable lengths which are bundled together within another tube and the process is repeated again and again to achieve the desired fibre diameter. Extrusion, swaging, rolling or drawing processes are used to produce *in situ* composites mechanically. The volume fraction of the fibre material is usually kept at 20 vol % or lower so that the fibres are isolated in the matrix and the matrix retains its desirable properties such as thermal and electrical conductivity.

Many investigations of the mechanical properties of *in situ* composites have been performed and the results were often compared with the rule of mixtures. In the rule of mixtures, stresses in the individual phases are added together in proportion to the volume fraction of each phase to give the composite stress. The strengths of the composites usually have had positive deviations from the rule of mixtures. A possible cause of this phenomenon has been proposed to be the role of the filament interfaces on strengthening [13, 14]. Body centred cubic (b c c) filaments were greatly effective in increasing the strength of deformation-processed composites because a ribbon-like cross-section was formed by the $\langle 1\,1\,0 \rangle$ fibre texture of the b c c filaments [15].

Recently, the tensile strengths of deformation-processed composites have been shown to correlate with filament spacings [16], leading to a Hall–Petch type relationship [17, 18]. Spitzig *et al.* [16] showed that the strength of heavily cold-worked Cu–Nb composite wires increased as the spacing between filaments decreased. It was found that the strength obeyed the Hall–Petch relationship. This suggests that the

0022–2461/91 $03.00 + .12

niobium filaments act as barriers to dislocation motion between the copper and niobium.

In this work three different iron powder sizes were used to investigate the strengthening effect in axisymmetrically deformation-processed Cu–20% Fe composites fabricated by a powder metallurgy process. After hot extrusion, these composites were swaged and drawn to wires at room temperature. The strengths were correlated with various factors; initial filament powder sizes, filament spacings and draw ratios. The strength of a Cu–20% Fe composite was compared with that of a similarly prepared Cu–20% Nb composite.

2. Experimental procedure

The copper powder used was gas atomized in the presence of a small partial pressure of oxygen, then reduced. The mean size of the copper powder was about 14 μm as evaluated by X-ray turbidimetry. The iron powder was fabricated by water atomization. This powder was sieved to obtain three different powder size ranges for three different Cu–20% Fe compacts as shown in Table I.

The copper and iron powders were mixed (Cu–20 vol % Fe) and processed as follows.

1. Powder placed in stainless steel can. $\varepsilon_s = \rho/\rho_{th} = 0.4$ (relative density = measured density/theoretical density).
2. Evacuated overnight under dynamic vacuum at 150 °C.
3. Temperature increased from 150 to 675 °C over 4 to 5 h under flowing hydrogen. This was done slowly to remove liquids in the powders.
4. Held 4 h at 675 °C under flowing hydrogen.
5. Cooled to room temperature under flowing hydrogen.
6. Hydrogen purged off with helium and back-filled with helium.
7. Transferred to glovebox and removed from can. $\varepsilon_s = 0.5$.
8. Bagged and evacuated under dynamic vacuum overnight and sealed.
9. Pressed at 380 MPa with 2 min hold time. $\varepsilon_s = 0.84$.
10. Back to glovebox, rebagged and evacuated overnight.
11. Repressed at 620 MPa. $\varepsilon_s = 0.95$.

TABLE I Iron powder size characteristics

Billet name	Iron powder size range		wt % of size in μm	
	Mesh	μm	μm	wt %
A	−80/+140	105–177	149–177	26.5
			125–149	39.4
			105–125	34.1
B	−140/+230	63–105	88–105	27.1
			74–88	38.5
			63–74	34.4
C	−270	<53	44–53	26.8
			37–44	28.3
			<37	44.9

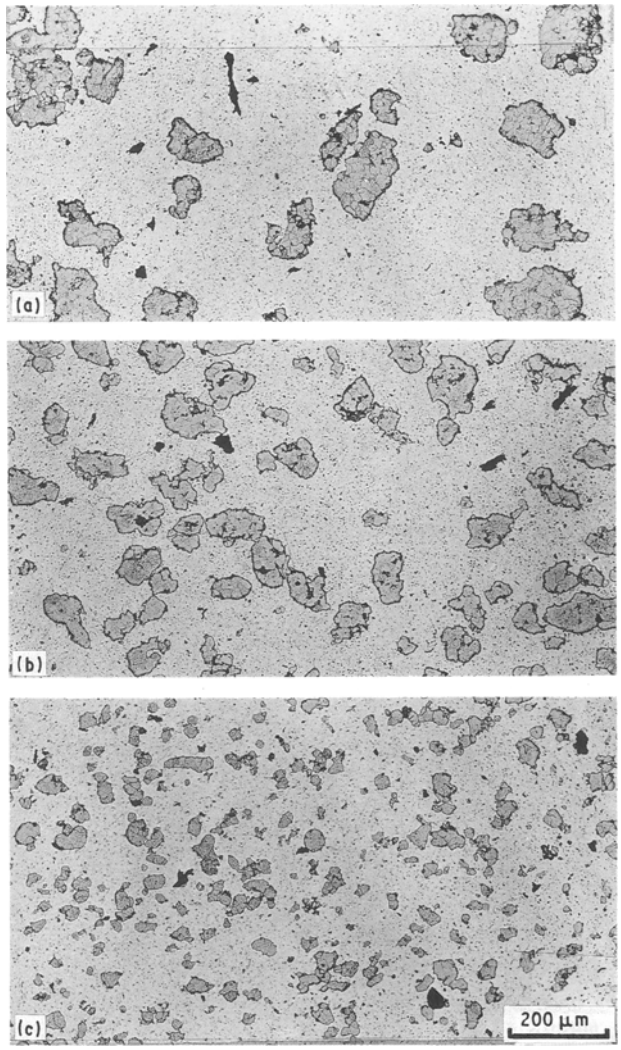

Figure 1 Optical micrographs of the Cu–20% Fe; (a) billet A, (b) billet B and (c) billet C.

The microstructures of the three Cu–20% Fe billets after cold isostatic pressing are shown in Fig. 1.

The billet size was about 7.5 cm diameter and 20 cm long. The three billets were put into pure copper cans and then sealed shut by electric arc welding. These billets were put in a furnace for 2.5 h at 500 °C and then hot extruded to 2 cm diameter rods. At this point the relative density was 99% and it was considered that this was the starting point for evaluating the effect of deformation processing on strengthening.

The extruded bars were reduced to a diameter of about 0.79 mm by cold swaging at room temperature. The direction of swaging was reversed after each pass to remove the spiral nebula structure in transverse sections [19]. The copper jacket was mechanically removed when the wire diameter was 1.27 cm. Then the wire was reduced to a diameter of about 0.15 mm by drawing through successive dies at room temperature. The dies were held in a vice and the wire was manually pulled through the dies. The wire ends were etched in a solution of 50% HNO_3 and 50% H_2O for starting through the dies.

The smallest wire diameter corresponds to a drawing strain of $\eta = 9.6$ or a reduction of area of 99.993% using the extruded bar as the starting point. Drawing

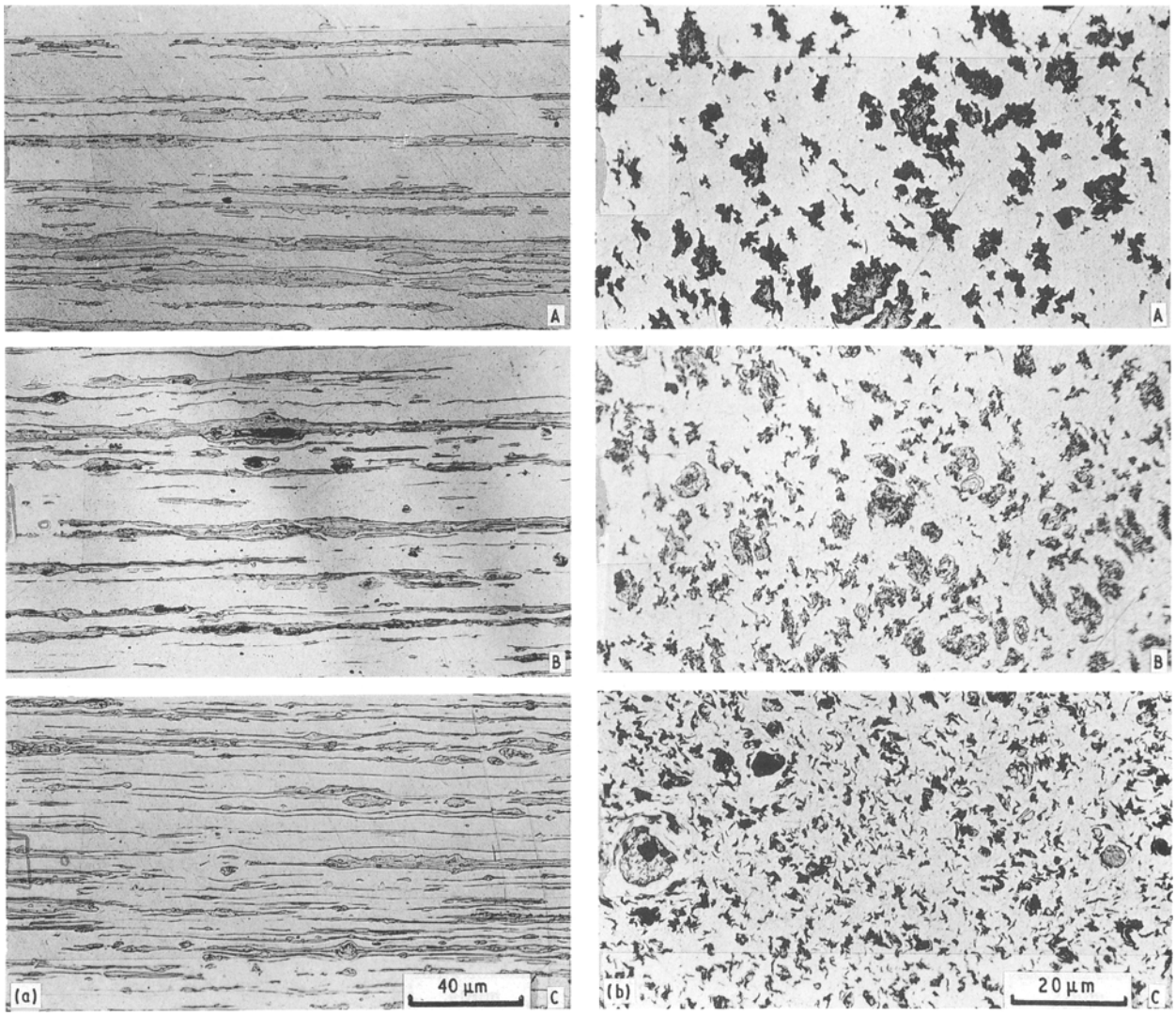

Figure 2 Optical micrographs of the Cu–20% Fe A, B and C composite wires drawn to an $\eta = 3.6$, 3.6 and 3.3, respectively. (a) Longitudinal sections, (b) transverse sections.

reductions will be given in terms of logarithmic strain by

$$\eta = \ln(A_0/A) \quad (1)$$

where A_0 is the area after the hot extrusion and A is the final cross-section area. Fig. 2 shows the characteristic morphology of the longitudinal and the transverse sections of Cu–20% Fe composites A, B and C wires that were drawn to an $\eta = 3.6$, 3.6 and 3.3, respectively. The longitudinal sections show that iron powders adopt a filamentary morphology during drawing. The transverse sections show the ribbon-like morphology of the filaments.

Tensile specimens were machined from the hot-extruded rods and wires drawn down to 1.6 mm diameter. For smaller diameter wires, tensile specimens were made by embedding the wire ends into copper sleeves using a superbond adhesive. All tensile specimens were tested at 295 K with a nominal strain rate of $1.7 \times 10^{-4}\,\text{sec}^{-1}$. A 2.5 cm strain gauge extensometer with a strain resolution of 5×10^{-3} was used for elongation measurements on specimens with diameters down to 0.4 mm. Filament spacings were determined by using standard stereological intercept procedures [20]. Fracture surfaces of the tensile specimens were examined in a scanning electron microscope to characterize fracture behaviour.

3. Results

Fig. 3 shows the true stress–true strain curves for Cu–20% Fe wires from the three different billets after drawing to various draw ratios up to $\eta = 9.6$. From these curves it is seen that the uniform elongation does not vary much with cold working from the minimum draw ratio, $\eta = 3.6$, to the maximum draw ratio, $\eta = 9.6$. It is also apparent that the strength at a given draw ratio is increased by decreasing the initial iron powder sizes, particularly at the higher draw ratios. The slope of the elastic line in Fig. 4 is 145 GPa, which is similar to the calculated value based on the rule of mixtures (146 GPa). The Young's modulus of the Cu–20% Fe did not appear to change with deformation strain at the lower draw ratios where the specimen size was sufficient for measurement using a clip-on strain gauge extensometer.

Fig. 4 compares the effect of draw ratio on the ultimate tensile stress of Cu–20% Fe composites from

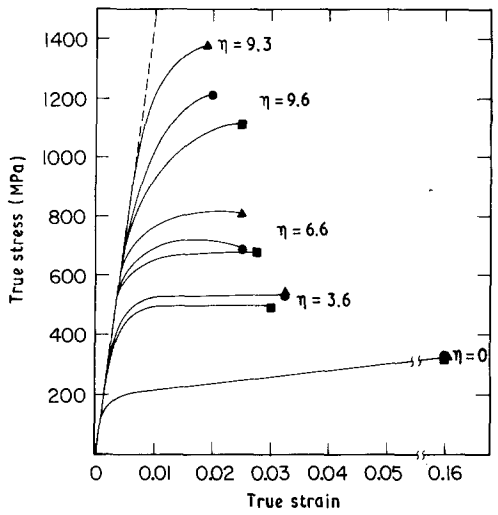

Figure 3 True stress–true strain curves of the different Cu–20%Fe billets at various draw ratios (η). Billets (■) A, (●) B, (▲) C.

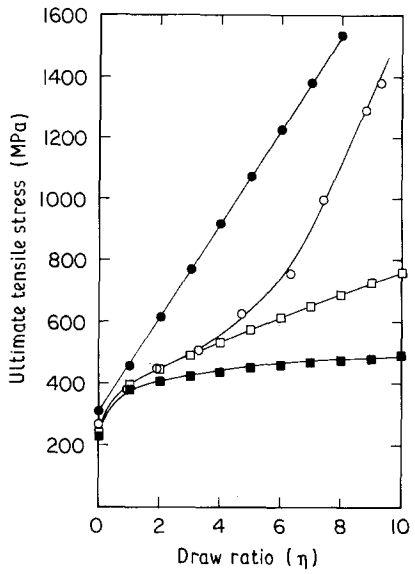

Figure 5 The ultimate tensile stress of the Cu–20% Fe C composite as compared with the calculated rule of mixtures stress as a function of the draw ratio. Data for iron and copper were taken from the literature [23]. (■) Pure copper, (●) pure iron, (□) Cu–20% Fe of ROM, (○) Cu–20% Fe C.

the three different iron powder size groups. The results for Cu–20% Nb composites fabricated by powder metallurgy processing [5] are also shown in this figure for comparison. The ultimate tensile stress was used as a measure of strength because it was well defined. The variation of strength with draw ratio becomes exponential in nature and shows no signs of levelling off at the higher draw ratios as does the strength of copper (see Fig. 5). It appears that at a similar filament size the strength of Cu–20% Fe is higher than that of Cu–20% Nb. This is expected because the shear modulus of iron (81.6 GPa) is larger than that of niobium (37.5 GPa) [21] and it has been shown that strength increases as the filament modulus increases [22]. The Cu–20% Fe composite made using the smallest iron powder sizes (< 53 μm) is shown to result in the greatest increase of strength. A similar result was observed for Cu–20% Nb and Cu–20% Ta composites when the initial dendrite size of the niobium and tantallum was reduced [22].

Fig. 5 is a comparison of the strength of the Cu–20% Fe composite fabricated from the smallest iron powder size with the strength calculated by the rule of mixtures (ROM). The ultimate tensile stress of the heavily cold-worked composite is anomalously increased as compared to the rule of mixtures. The rule of mixtures stresses were calculated using previously proposed strength values for copper and iron [23] by

$$\sigma_{Fe} = 310 + 153\eta_{Fe}\,(\text{MPa}) \quad (2)$$

$$\sigma_{Cu} = 224 + 153\eta_{Cu}^{0.24}\,(\text{MPa}) \quad (3)$$

$$\sigma_c = V_{Fe}\sigma_{Fe} + V_{Cu}\sigma_{Cu} \quad (4)$$

where σ_c, σ_{Fe} and σ_{Cu} are the ultimate tensile stresses of the composite, iron filaments and copper matrix, V_{Fe} and V_{Cu} are the volume fractions of iron and

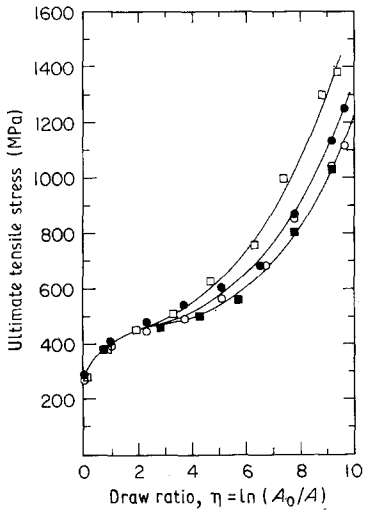

Figure 4 Effect of draw ratio (η) and the iron powder size on the ultimate tensile stress of the (○, ●, □) Cu–20% Fe and (■) Cu–20% Nb composites. (○) A, 105 to 177 μm Fe; (●) B, 63 to 105 μm Fe; (□) C, < 53 μm Fe; (■) 88–125 μm Nb.

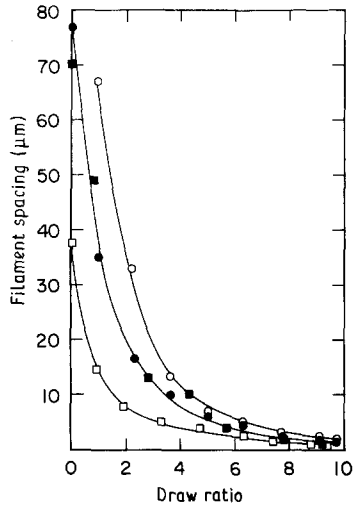

Figure 6 Effect of the draw ratio (η) and the iron powder size on the filament spacings (λ) in the (○, ●, □) Cu–20% Fe and (■) Cu–20% Nb composites. For key, see Fig. 4.

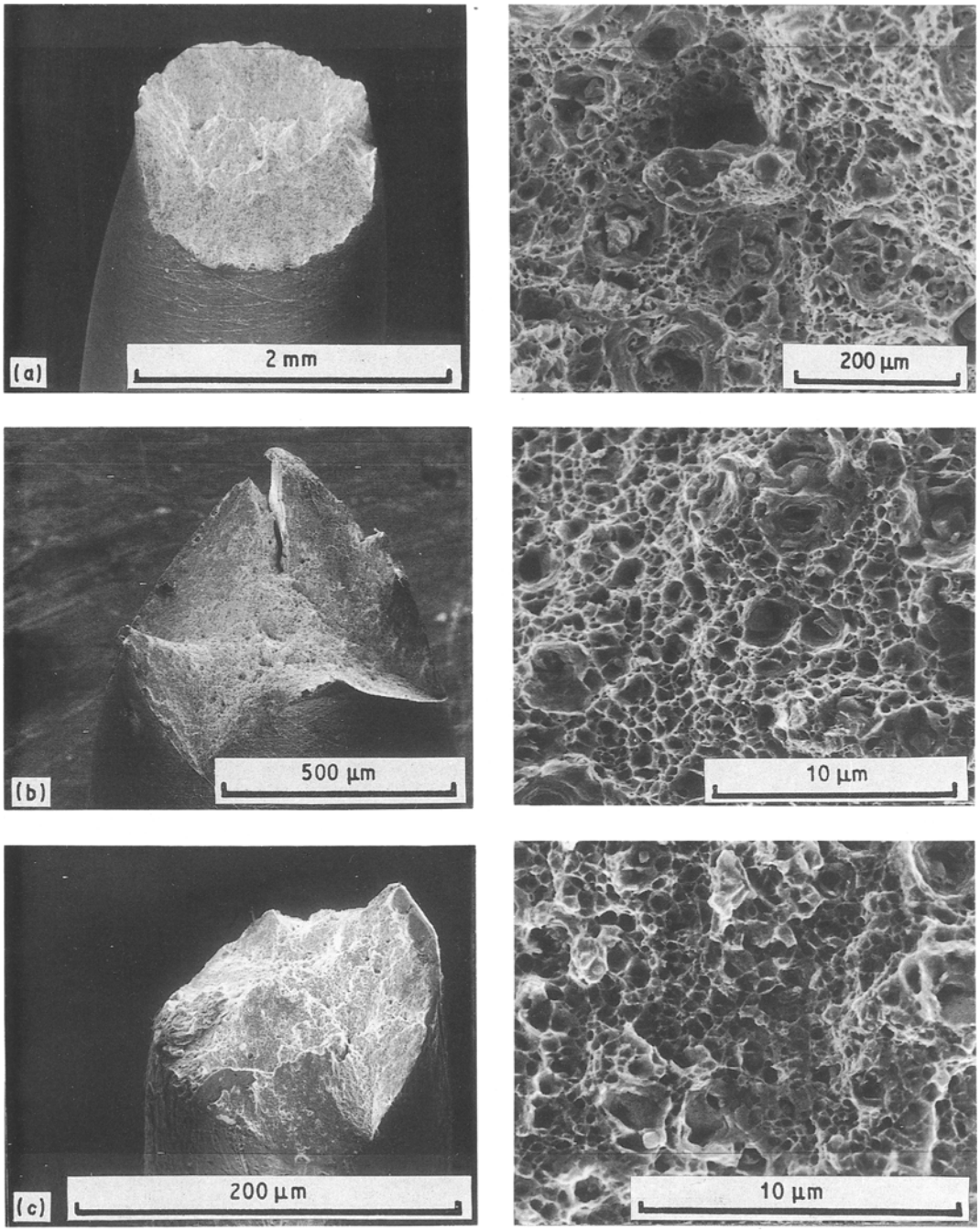

Figure 7 SEM images of fracture surfaces of the Cu–20%Fe C composite drawn to draw ratios (a) $\eta = 3.3$, (b) $\eta = 6.3$ and (c) $\eta = 8.8$ and tested at room temperature.

copper, and η_{Fe} and η_{Cu} are the true strains of iron and copper, respectively.

The effect of draw ratio on the spacing (λ) of the iron filaments in the Cu–20% Fe composites is shown in Fig. 6. The spacings decrease with increasing wire reduction. The composites with the smaller iron powder sizes had the smaller spacings at a given draw ratio throughout the wire processing. The Cu–20% Fe B and Cu–20% Nb composites which had similar initial powder sizes for iron and niobium, respectively, appeared to have similar spacings at the different draw ratios.

The fracture surfaces of Cu–20% Fe C composite specimens tested at room temperature, are shown in Fig. 7. The three different ratios shown, $\eta = 3.3$, 6.3 and 8.8, represent the changes in fracture behaviour observed in the composite. The fracture surfaces of the Cu–20% Fe composites A and B were similar to C. The fractures at the lower draw ratios ($\eta \leq 5.0$) were of the ductile "cup and cone" type, as shown in Fig. 7a. The fractures at draw ratios of $\eta = 6.3$ and 8.8 showed predominantly shear character as indicated in Fig. 7b and c. This change in fracture behaviour shown in Fig. 7a–c occurs as strengthening in the composites becomes pronounced, as shown in Fig. 5. Dimples were observed on the fracture surfaces of all the specimens and iron filaments were found within them by X-ray analysis in the scanning electron microscope.

The dimple size decreased as the draw ratio increased as expected, because the iron filament spacing decreased with increasing draw ratio.

4. Discussion

The maximum ultimate tensile stresses obtained for the deformation-processed Cu–20% Fe can be compared with previous results on Cu–Fe composites. Cu–15% Fe composites made by arc melting followed by deformation processing of the ingots measured maximum increases in strength over the rule of mixtures values of about 350 MPa [23]. This is about one-half of the value shown in Fig. 5 for the Cu–20% Fe composite C deformation processed to $\eta = 9.2$. However, in this previous study heat treatments were used during processing in attempts to separate out matrix and filament contributions to strengthening but the minimum filament spacing was about 1.2 μm which is closer to that of Cu–20% Fe B composite. This composite had an increase of 500 MPa above that predicted by the rule of mixtures after deformation processing to $\eta = 9.6$. Other work on Cu–20% Fe composites formed by melting procedures followed by deformation processing showed maximum ultimate tensile strengths of 1250 MPa but no data were given on filament spacings [24]. Previous results on Cu–25% Fe composites formed by a bundling and drawing technique starting with wires of iron inserted into copper tubes showed maximum ultimate tensile stresses near 620 MPa [12]. Comparison of the present results on the powder processed Cu–20% Fe composites with these previous data shows that the powder processing route for fabricating the initial compacts results in strengths equivalent to or better than those reported for ingot-cast compacts. Comparison with compacts formed by inserting wires of one component into another followed by bundling and drawing shows the advantage of starting with a powder metallurgy compact or casting of the alloy for producing high-strength material.

Fig. 8 shows the correlation between ultimate tensile stresses and filament spacings (λ) for the Cu–20% Fe composites by replotting the data of Figs 4 and 6 on a logarithmic graph. The lines in Fig. 8 are parallel to each other. One line was drawn through the data

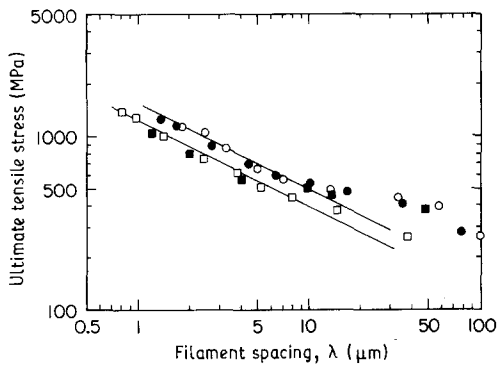

Figure 8 Ultimate tensile stress according to the initial powder size and filament spacings (λ) of the (○, ●, □) Cu–20% Fe and (■) Cu–20%Nb composites. For key, see Fig. 4.

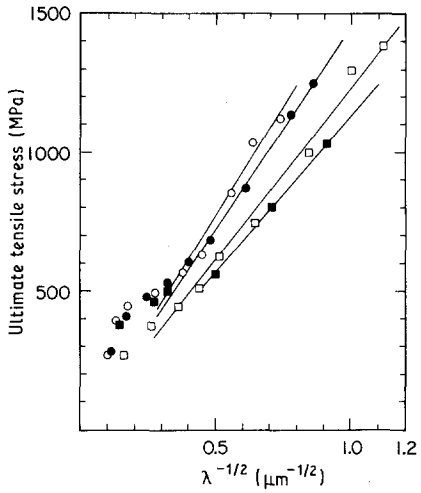

Figure 9 Ultimate tensile stress according to the initial powder size and $(\lambda)^{-1/2}$ of the (○, ●, □) Cu–20% Fe and (■) Cu–20% Nb composites. For key, see Fig. 4.

for Cu–20% Fe A and B, and another line through the data for Cu–20% Fe C and Cu–20% Nb. The slope of the lines in Fig. 8 is about −0.49 which is similar to the exponential constant (−0.5) of the Hall–Petch relationship.

To demonstrate more clearly the Hall–Petch relationship the ultimate tensile stresses are plotted against $\lambda^{-1/2}$ in Fig. 9. As can be seen, a good correlation with this relationship is shown for all of the composites when the filament spacings are less than approximately 10 μm. The slopes of lines are different from one another and increase as the initial iron powder size increases which indicates that the strength does not solely depend on the filament spacings in powder metallurgy processed composites as was also demonstrated in arc-cast Cu–20% Nb and Cu–20% Ta composites [22]. The strength of the larger iron powder size composites is higher than that of the smaller iron powder size composites at a given filament spacing. This is an expected result, because the larger iron powder size composites need more deformation processing to reach the particular value of the filament spacing as compared with the smaller iron powder size composite. This shows that the slope (k) of the Hall–Petch relationship is related to the initial filament powder size of composites, in accord with results in Cu–20% Nb and Cu–20% Ta composites [22]. Therefore, the effect of decreasing initial powder size on strengthening is the same as that of decreasing initial dendrite size. As will be discussed later, the strength of the Cu–20% Fe composites obeys the rule of mixtures at the larger filament spacings. However, the strength of these composites obeys the Hall–Petch relationship after smaller degrees of deformation processing as the initial powder size becomes smaller.

The Hall–Petch equation has the form

$$\sigma = \sigma_0 + k\lambda^{-1/2} \quad (5)$$

where σ is the ultimate tensile stress, σ_0 is the stress required to move dislocations in the matrix and filaments, and λ is the filament spacing. The intercept stress in Fig. 9 is σ_0 and is not very significant because

it is near to 0 MPa using extrapolations of the lines of all composites to $\lambda^{-1/2}$ equal to zero. However, if the strength of these composites also obeys a Hall–Petch relationship at larger filament spacings (over about 10 μm in this research), the intercept stress becomes significant. However, at the larger filament spacings many grains occur between filaments and grain boundaries themselves can become obstacles leading to an intercept stress. Therefore, the intercept stress is expected to change with deformation processing until the filament spacings, rather than the grains between the filaments, control strengthening. The same phenomenon was also observed in a previous study of powder metallurgy processed Cu–20% Nb composites [5]. In addition, from Figs 4 and 6 it is apparent that the ultimate tensile stresses of the Cu–20% Fe composites are similar to each other at the lower deformation strains where the filament spacings are greater than about 10 μm. The tensile strengths of the Cu–20% Fe composites which have these larger filament spacings may be primarily determined by a rule of mixtures that simply expresses the strength of the composite in terms of its components (Equation 4). This is apparent in Fig. 5 which shows that the strength of the Cu–20% Fe C composite is in good agreement with a rule of mixtures at low draw ratios, i.e. large filament spacings.

The tensile strength at smaller filament spacings where Hall–Petch behaviour is observed will be considered for comparison of the initial filament powder size and the shear modulus of the composites on strengthening. Fig. 10 shows the ultimate tensile stress dependence on the normalized filament spacings $[(\lambda/\lambda_0)^{-1/2}]$ obtained by dividing the filament spacings by the initial filament spacings of the Cu–20% Fe and Cu–20% Nb composites after hot extrusion. As can be seen, the strength of every composite still linearly depends on $(\lambda/\lambda_0)^{-1/2}$ and the slope of the lines increases as the initial iron powder size decreases. These results show the importance of decreasing the initial filament powder size as much as possible for increasing the strength of composites fabricated by powder metallurgy methods.

The critical filament spacing where the Hall–Petch equation strength (σ) is more dominant than the rule of mixtures strength (σ_{ROM}) can be calculated by using the following equations

$$\sigma_{ROM} = 241.2 + 30.6(\eta + 4\eta^{0.24}) \quad (6)$$

$$\sigma = k\lambda^{-1/2}, \quad k_A = 1550, \quad k_B = 1450$$

$$\text{and } k_C = 1230 \ (\text{MPa } \mu\text{m}^{1/2}) \quad (7)$$

$$\lambda/\lambda_0 = 0.45\exp(-0.34\eta),$$

$$\lambda_0(A) = 101, \quad \lambda_0(B) = 77.2$$

$$\text{and } \lambda_0(C) = 37.5 \ (\mu\text{m}) \quad (8)$$

where Equations 6, 7 and 8 are obtained from Equation 4, Fig. 9 and the data in Fig. 6, respectively. The calculations show that the filament spacing must be less than about 6.5 μm to obey the Hall–Petch relationship rather than the rule of mixtures, as shown in Table II. Therefore, if the initial filament spacing were less than 6.5 μm, σ would be expected to be higher than σ_{ROM} from the beginning of the deformation processing.

In a previous study [16], it was suggested that the primary function of the niobium filaments was to provide closely spaced barriers to dislocation glide in copper and the effectiveness of the filament interfaces as dislocation barriers could be related to the filament strength. This suggestion also applies to the Cu–Fe composites as has been shown in Figs 9 and 10. This appears reasonable because in dislocation models [25] used to derive the Hall–Petch relationship the interaction between a screw dislocation in a matrix and a lamellar defect, such as a filament, depends on the relative values of shear moduli of the matrix and the defect [14]. Thus, the strength of the Cu–20% Fe B composite is expected to be higher than that of the Cu–20% Nb composite, because the modulus of iron (81.6 GPa) is higher than that of niobium (37.5 GPa).

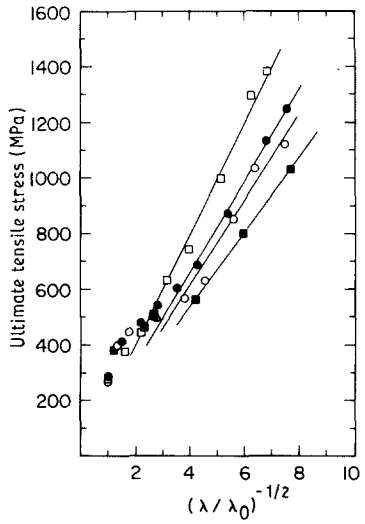

Figure 10 Ultimate tensile stress according to the initial filament powder size and normalized filament spacing ($(\lambda/\lambda_0)^{-1/2}$, where λ_0 is the filament spacing after hot extrusion) of the (○, ●, □) Cu–20% Fe and (■) Cu–20% Nb composites. For key, see Fig. 4.

TABLE II Results of calculation

η	Composite	λ(μm)	σ(MPa)	σ_{ROM}(MPa)	Remarks
2	A	23.03	323.0	447.0	
	B	17.60	338.5		
	C	8.55	420.7		
3	A	16.39	382.9		At η = 2.9
	B	12.53	409.7		λ_C = 6.30
	C	6.09	498.6		σ = 490.2
					σ_{ROM} = 488.0
4	A	11.67	453.8	534.3	
	B	8.92	485.6		
	C	4.33	591.0		
5	A	8.30	537.9	574.3	
	B	6.35	575.6		
	C	3.08	700.5		
6	A	5.91	637.6	613.0	At η = 5.7
	B	4.52	682.2		λ_A = 6.54
	C	2.19	830.4		σ = 605.9
					σ_{ROM} = 601.5

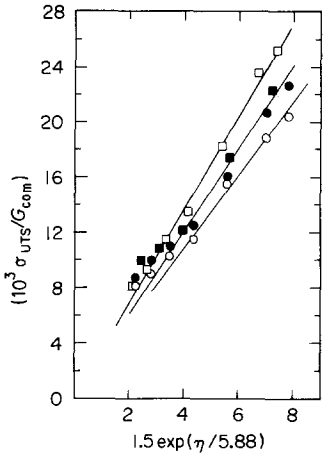

Figure 11 Ultimate tensile stress dependence on the draw ratio, the composite shear modulus (G_{com}) and the initial filament powder size of the (○, ●, □) Cu–20% Fe and (■) Cu–20% Nb composites. For key, see Fig. 4.

For linear pile-ups in a two-phase medium, the slope (k) in the Hall–Petch equation is related to the shear moduli of the two phases by

$$k \approx [(1 + K)/(1 - K)^{1/2}] \quad (9)$$

where $K = (G_2 - G_1)/(G_2 + G_1)$ and is defined in the range of $0 \leq K < 1$, and G_1 and G_2 are the shear moduli of the matrix and the barrier, respectively [14]. Treating the filament as the barrier the ratio of k values for the Cu–Fe and Cu–Nb composites is expected to be 1.3, which is similar to the ratio of slopes for the Cu–20% Fe B and Cu–20% Nb composites from Fig. 9, which is 1.28.

The data in Fig. 10 were replotted in Fig. 11 by dividing the ultimate tensile stresses of the composites by the composite shear modulus (G_{COM}) and substituting for λ/λ_0 in Equation 8. The composite shear moduli were calculated by using the rule of mixtures, Poisson's ratio and Young's modulus of copper, iron and niobium in the literature [21]. The shear moduli of Cu–20% Fe and Cu–20% Nb are 54.8 and 46.0 GPa, respectively. On this normalized plot, the strengths of the Cu–20% Nb and Cu–20% Fe composites of similar initial niobium and iron powder sizes, respectively, are in good agreement.

The results of Figs 10 and 11 show that a good correlation exists between the strength of the composite and the experimentally controlled parameters such as the initial filament powder size, the draw ratio and the filament material. To obtain optimum strengthening in deformation-processed composites it is important to use a high draw ratio, a filament material with a large shear modulus and a small filament powder size in the original compact. Similar conclusions were reached for Cu–20% Nb and Cu–20% Ta composites [22].

5. Conclusion

Three Cu–20% Fe composites with different iron powder sizes were fabricated using powder metallurgy processes. The strength of powder metallurgy processed Cu–20% Fe deformation-processed composites at room temperature was anomalously increased by increasing draw ratio (η). The strength increase obeyed the Hall–Petch relationship at smaller filament spacings, but the strength was more in accord with a rule of mixtures equation at filament spacings greater than about 6.5 μm. After equivalent deformation processing the strengths of the composites increased with decreasing initial iron powder size.

Comparison of the strengths of the Cu–20% Fe and Cu–20% Nb [5] composites which had similar initial filament powder sizes showed that Cu–20% Fe was stronger after identical degrees of deformation processing. This was explained by the effectiveness of the filament interfaces as dislocation barriers being related to the shear modulus of the filament. Thus, it appears to be important for increasing the strength of deformation-processed composites to use a filament material that has a large shear modulus.

Acknowledgements

We thank L. K. Reed for experimental assistance, H. H. Baker for metallographic work and C. L. Trybus for billets preparation. This work was performed at Ames Laboratory under contract no. W-7402-eng-82 with the US Department of Energy. This research was supported by the Director of the Energy Research, Office of Basic Energy Sciences.

References

1. N. P. CHEREMISINOFF and P. N. CHEREMISINOFF, "Fiberglass-Reinforced Plastics Deskbook" (Ann Arbor Science, Ann Arbor, Michigan, 1978) Ch. 1.
2. K. M. RALLS, T. H. COURTNEY and J. WULFF, "Introduction to Materials Science and Engineering" (Wiley, New York, 1976) p. 400.
3. B. D. AGARWAL and L. J. BROUTMAN, "Analysis and Performance of Fiber Composites" (Wiley, New York, 1980) Ch. 1.
4. T. A. NIELSON, MS thesis, Michigan Technological University (1982).
5. C. L. TRYBUS, W. A. SPITZIG, J. D. VERHOEVEN and F. A. SCHMIDT, in "Powder Metallurgy Composites", edited by P. Kumar, K. Vedula and A. Ritter (The Metallurgical Society, Warrendale, Pennsylvania, 1988) p. 97.
6. Y. D. YAO and S. FONER, *Appl. Phys. Lett.* **43** (1983) 697.
7. G. FROMMEYER and G. WASSERMANN, *Acta Metall.* **23** (1975) 1353.
8. D. G. KUBISCH and T. H. COURTNEY, *Met. Trans.* **17A** (1986) 1165.
9. J. D. VERHOEVEN, F. A. SCHMIDT, E. D. GIBSON and W. A. SPITZIG, *J. Metals* **38** (9) (1986) 20.
10. J. D. VERHOEVEN, E. D. GIBSON, F. A. SCHMIDT and D. K. FINNEMORE, *J. Mater. Sci.* **15** (1980) 1449.
11. F. D. LEVI, *J. Appl. Phys.* **31** (1960) 1449.
12. G. GARMONG and L. A. SHEPARD, *Met. Trans.* **2** (1971) 175.
13. B. J. SHAW, *Acta Metall.* **15** (1967) 1169.
14. Y. T. CHOU, *Canad. J. Phys.* **45** (1967) 559.
15. J. BEVK, J. P. HARBISON and J. L. BELL, *J. Appl. Phys.* **49** (1978) 6031.
16. W. A. SPITZIG, A. R. PELTON and F. C. LAABS, *Acta Metall.* **35** (1987) 2427.
17. N. J. PETCH, *J. Iron Steel Inst.* **174** (1953) 25.
18. E. O. HALL, *Proc. Phys. Soc. Lond.* **B64** (1951) 747.

19. W. A. SPITZIG, P. D. KROTZ, L. S. CHUMBLEY, H. L. DOWNING, and J. D. VERHOEVEN, *Mater. Res. Soc. Symp. Proc.* **120** (1988) 45.
20. E. E. UNDERWOOD, "Quantitative Stereology" (Addison-Wesley, Reading, Massachusetts, 1970) Chs 3 and 4.
21. M. A. MEYERS and K. K. CHAWLA, "Mechanical Metallurgy" (Prentice Hall, Englewood Cliffs, New Jersey, 1984) Chs 1 and 12.
22. W. A. SPITZIG and P. D. KROTZ, *Acta Metall.* **36** (1988) 1709.
23. P. D. FUNKENBUSCH and T. H. COURTNEY, *Scripta Metall.* **15** (1981) 1349.
24. J. D. VERHOEVEN, S. C. CHUEH and E. D. GIBSON, *J. Mater. Sci.* **24** (1989) 1748.
25. R. W. ARMSTRONG, in "Yield, Flow and Fracture of Polycrystals", edited by T. N. Baker (Applied Science, New York, 1983) Ch. 1.

Received 21 August 1989
and accepted 19 February 1990